The Journal of Immunology

Characterization of a Transitional Preplasmablast Population in the Process of Human B Cell to Plasma Cell Differentiation

Michel Jourdan, Anouk Caraux, Gersende Caron, Nicolas Robert, Geneviève Fiol, Thierry Rème, Karine Bolloré, Jean-Pierre Vendrell, Simon Le Gallou, Frédéric Mourcin, John De Vos, Alboukadel Kassambara, Christophe Duperray, Dirk Hose, Thierry Fest, Karin Tarte and Bernard Klein

J Immunol 2011; 187:3931-3941; Prepublished online 14 September 2011;
doi: 10.4049/jimmunol.1101230
http://www.jimmunol.org/content/187/8/3931

The Journal of Immunology is published twice each month by
The American Association of Immunologists, Inc.,
1451 Rockville Pike, Suite 650, Rockville, MD 20852

Print ISSN: 0022-1767 Online ISSN: 1550-6606.

Characterization of a Transitional Preplasmablast Population in the Process of Human B Cell to Plasma Cell Differentiation

Michel Jourdan,* Anouk Caraux,* Gersende Caron,[†,‡] Nicolas Robert,[§] Geneviève Fiol,[§] Thierry Rème,*[,§] Karine Bolloré,[§] Jean-Pierre Vendrell,[§,¶] Simon Le Gallou,[†] Frédéric Mourcin,[†] John De Vos,*[,§,¶] Alboukadel Kassambara,* Christophe Duperray,*[,§] Dirk Hose,[‖,#] Thierry Fest,[†,‡] Karin Tarte,[†,‡] and Bernard Klein*[,§,¶]

The early steps of differentiation of human B cells into plasma cells are poorly known. We report a transitional population of CD20$^{low/-}$CD38^{-} preplasmablasts along differentiation of human memory B cells into plasma cells in vitro. Preplasmablasts lack documented B cell or plasma cell (CD20, CD38, and CD138) markers, express CD30 and IL-6R, and secrete Igs at a weaker level than do plasmablasts or plasma cells. These preplasmablasts further differentiate into CD20^{-}CD38^{high}CD138^{-} plasmablasts and then CD20^{-}CD38^{high}CD138^{+} plasma cells. Preplasmablasts were fully characterized in terms of whole genome transcriptome profiling and phenotype. Preplasmablasts coexpress B and plasma cell transcription factors, but at a reduced level compared with B cells, plasmablasts, or plasma cells. They express the unspliced form of *XBP1* mRNA mainly, whereas plasmablasts and plasma cells express essentially the spliced form. An in vivo counterpart (CD19^{+}CD20$^{low/-}$CD38^{-}IL-6R^{+} cells) of in vitro-generated preplasmablasts could be detected in human lymph nodes (0.06% of CD19^{+} cells) and tonsils (0.05% of CD19^{+} cells). An open access "B to Plasma Cell Atlas," which makes it possible to interrogate gene expression in the process of B cell to plasma cell differentiation, is provided. Taken together, our findings show the existence of a transitional preplasmablast population using an in vitro model of plasma cell generation and of its in vivo counterpart in various lymphoid tissues. ***The Journal of Immunology*****, 2011, 187: 3931–3941.**

The production of high-affinity Ig-producing plasma cells (PCs) is the end product of a complex network of cell interaction, gene rearrangements, and mutations. Ag encounter induces both B and T cells to move to the outer T cell zone, in which they interact each other. Activated B cells then migrate to follicles and initiate a germinal center (GC) reaction characterized by an extensive centroblastic proliferation associated with random somatic hypermutation in Ig genes (1) that are dependent on activation-induced deaminase (AID). CXCR4^{+} centroblasts are found within the dark zone of the GC, in close contact with poorly characterized dark zone follicular dendritic cells (FDCs) that do not produce CXCL13 (CXCR5 ligand) but express high levels of CXCL12 (CXCR4 ligand) (2, 3). The internalization of CXCR4 after CXCL12 exposure allows the rapid CXCR5-dependent migration of centroblasts to the light zone, acquiring a centrocyte phenotype, and these centrocytes compete with each other for the capture of Ag presented as immune complexes by CXCL13^{+} light zone FDCs. B cells with high-affinity Ig will pick up greater amounts of Ag, thus receiving a BCR-mediated signal, together with a complex set of FDC-derived growth factors and adhesion molecules (3–5). FDC/B cell interaction is short-lived but allows the capture of Ag for further presentation to a specific subset of GC-restricted follicular helper T cells (T_{FH}). T_{FH} provide them with essential survival, class switch recombination, and differentiation signals, in particular CD40L and IL-21, that will contribute to the NF-κB/IRF4–dependent downregulation of BCL6 and the IRF4/STAT3-dependent upregulation of Blimp1. Owing to their lower affinity for Ag, the vast majority of centrocytes are not rescued by this FDC/T_{FH} system and are engulfed by tingible body macrophages (6). The GC is a dynamic structure, with GC B cells moving cyclically between the dark and light zones to undergo repeated rounds of mutation and selection (2, 7). A successful selection will eventually promote GC B cells to give rise to early Ig secreting plasmablasts (PBs) or memory B cells (MBCs) under presently unknown signals. MBCs persist after immunization both as Ag-dependent memory within residual GC-like

*INSERM, Unité 1040, 34000 Montpellier, France; [†]INSERM, Unité 917, 35043 Rennes, France; [‡]Pôle Cellules et Tissus, Centre Hospitalier Universitaire de Rennes, 35033 Rennes, France; [§]Centre Hospitalier Universitaire de Montpellier, Institut de Recherche en Biothérapie, 34295 Montpellier, France; [¶]Unité de Formation et de Recherche de Médecine, Université Montpellier 1, 34000 Montpellier, France; [‖]Medizinische Klinik und Poliklinik V, Universitätsklinikum Heidelberg, 69120 Heidelberg, Germany; and [#]Nationales Centrum für Tumorerkrankungen, D-69120 Heidelberg, Germany

Received for publication April 27, 2011. Accepted for publication August 3, 2011.

This work was supported by grants from the Ligue Nationale Contre le Cancer (équipe labellisée 2009), Paris, France, and from L'Institut National du Cancer (Grant RPT09001FFA).

M.J. and A.C. designed research, performed the experiments, and wrote the paper; K.T., T.F., G.C., F.M., and S.L.G. performed the experiments to characterize cells in vivo and corrected the paper; G.F. and N.R. provided technical assistance; K.B. and J.-P.V. performed ELISPOT assays; D.H. provided normal bone marrow samples; A.K. provided assistance for bioinformatics analysis; J.D.V. designed the Amazonia Web site and T.R. designed the RAGE Web site; C.D. provided assistance for cytometry experiments; and B.K. is the senior investigator who designed research and wrote the paper.

Address correspondence and reprint requests to Prof. Bernard Klein, INSERM, Unité 1040, Institut de Recherche en Biothérapie, Centre Hospitalier Universitaire de Montpellier, Hôpital Saint Eloi, Avenue Augustin Fliche, 34295 Montpellier, France. E-mail address: bernard.klein@inserm.fr

The online version of this article contains supplemental material.

Abbreviations used in this article: AID, activation-induced deaminase; BM, bone marrow; cy, cytoplasmic; D, day; FDC, follicular dendritic cell; GC, germinal center; MBC, memory B cell; ODN, oligodeoxynucleotide; PB, plasmablast; PC, plasma cell; prePB, preplasmablast; s, surface; SAM, significance analysis of microarray; sCD40L, soluble CD40L; SI, stain index; T_{FH}, follicular helper T cell; *XBP1*s, *XBP1* spliced; *XBP1*u, *XBP1* unspliced.

structures, in close contact to FDCs and T cells, and Ag-independent memory dispersed outside B cell follicles (8). In case of secondary immunization, MBCs can be restimulated to highly proliferate and differentiate into PBs and PCs.

The migration pattern of PBs has been recently documented in mice (9). PBs travel through the T cell zone toward the medullary cords. They are first found in the outer T cell zone close to $CD11c^{+}CD8\alpha^{-}$ dendritic cells, which highly produce IL-6. In vivo imaging has shown that PBs have a unique pattern of migration in T cell zone characterized by long linear paths that are randomly oriented (10). This migration pattern is dependent on an integrin ICAM1/2 axis and independent on a chemokine gradient. Once arrived in the medullary zone, PBs further differentiate in contact with $Gr1^{+}CD11b^{+}F4/80^{+}$ monocytes/macrophages that highly produce CXCL12, APRIL, and IL-6 (9). PBs are retained in the medullary zone by the CXCL12 gradient but still keep moving. One putative reason of this continuous moving is to be able to share the limiting PC niche. Most PBs will die in medullary cords, and the surviving ones will exit the lymph node into lymphatic vessels through a SP1-dependent gradient (11) and enter the blood circulation in which they survive for a short period unless they can find a survival niche either in the bone marrow (BM), spleen, or mucosa-associated lymphoid tissues, in which they further differentiate into long-lived PCs (12).

Several studies have contributed to better understand the process of differentiation of human centrocytes or MBCs into PBs and then mature PCs (reviewed in Ref. 13). The usual features of PBs are cell cycling, Ig secretion, high CD38 expression, and loss of B cell markers unlike CD19 (14–16). Those of mature PCs are stop in cell cycle, Ig secretion, high CD38 expression, and CD138 proteoglycan expression (17). We have shown that tonsil-purified $CD20^{+}CXCR4^{-}CXCR5^{+}$ centrocytes already express PC transcription factors (IRF4, Blimp-1, XBP1) together with B cell transcription factors (BCL6, PAX5), although it is not clear whether centrocytes are a heterogeneous cell population containing centrocytes and cells already committed to PC differentiation (18). In an elegant study using cellular affinity matrix technology to capture secreted Igs, Arce et al. (19) have shown the existence of a minor population of $CD38^{-/low}$ Ig-secreting cells in tonsils together with classical $CD38^{high}$ Ig-secreting cells. $CD38^{-/low}$ cells weakly expressed CD27 compared with $CD38^{high}$ cells. The $CD38^{-/low}$ Ig-secreting cells were not detected in the peripheral blood or BM. They were thought to be the precursors of $CD38^{high}$ Ig-secreting cells in an in vitro model of B cell differentiation using PBMCs and tetanus toxoid activation. $CD38^{-/low}$ Ig-secreting cells were also reported in another model of B cell differentiation mimicking T cell help deploying CD40L, IL-2, and IL-10 activation of MBCs (20). Given their poor ability to survive upon CD40 activation removal, these $CD38^{-/low}$ Ig-secreting cells were initially assumed to be early precursors of short-term surviving plasma cells (20). In a following study, this group has shown that the ability to secrete Igs was mainly restricted to $CD27^{high}$ cells, independently of CD38 expression (21).

Using a similar model of PC generation based on initial CD40L and oligodeoxynucleotide (ODN) activation of MBCs, we show in this study that $CD38^{-}CD20^{-/low}CD27^{low}$ Ig-secreting cells (termed preplasmablasts, prePBs) precedes the generation of $CD38^{high}CD27^{high}$ PBs and then PCs. PrePBs fully survive and differentiate into PBs and PCs upon removal of CD40 activation. A full molecular and phenotypic characterization of prePBs is provided, showing that these cells express specifically CD30, IL-6R, and cytoplasmic Igs, express weakly CD27, do not express B cell or PC markers (CD38 and CD138), and secrete Igs at a lower level than do PBs or PCs. The in vivo counterpart of these prePBs could be found in various lymphoid tissues.

Materials and Methods

Reagents

Human recombinant IL-2 and IFN-α were purchased from R&D Systems (Minneapolis, MN), IL-6 and IL-15 were from AbCys (Paris, France), and IL-10 was from PeproTech (Rocky Hill, NJ). Mouse (or rat when indicated) mAbs conjugated to Alexa Fluor 488, Alexa Fluor 647, allophycocyanin, allophycocyanin-H7, allophycocyanin-Cy7, FITC, PerCP-Cy5.5, PE, and PE-Cy7 specific for human CD19 (clones HIB19 and SJ25C1), CD24 (clone ML5), CD27 (clones L128 and M-T271), CD30 (clone BerH8), CD38 (clone HIT2), CD43 (clone 1G10), CD45 (clone HI30), CD138 (clone MI15), CXCR5 (clone RF8B2), IgG (clone G18-145), IgM (clone G20-127), and Ki67 (clone B56) were purchased from BD Biosciences (Le Pont De Claix, France); CD20 (clone B9E9), CD126 (IL-6R, clone M91), and CD138 (clone B-A38) from were Beckman Coulter (Fullerton, CA); CCR10 (rat, clone 314305) was from R&D Systems; and IgG (polyclonal goat Ab) was from SouthernBiotech (Birmingham, AL).

Cell samples

Peripheral blood cells from healthy volunteers were purchased from the French Blood Center (Etablissement Français du Sang Pyrénnées-Méditérannée, Toulouse, France). After removal of $CD2^{+}$ cells using anti-CD2 magnetic beads (Invitrogen, Cergy Pontoise, France), $CD19^{+}CD27^{+}$ MBCs were sorted with a multicolor fluorescence FACSAria device with a purity $\geq$ 95% (see Fig. 1A). Cells produced in the culture system were FACS-sorted using FITC-conjugated anti-CD20 mAb and PE-conjugated anti-CD38 mAb for day (D) 4 $CD20^{high}CD38^{-}$ cells, D4 $CD20^{low}CD38^{-}$ cells, and D4 $CD20^{-}CD38^{-}$ cells, as well as D7 PBs ($CD20^{-}CD38^{+}$). D10 PCs ($CD20^{-}CD138^{+}$) were FACS-sorted using FITC-conjugated anti-CD20 mAb and PE-conjugated anti-CD138 mAb. The purity of FACS-sorted cell populations was $\geq$95% as assayed by cytometry. We looked for prePBs in tonsil, lymph node, BM, and peripheral blood samples. Tonsils were obtained from routine tonsillectomies performed at Chidren's Clinique La Sagesse at Rennes (France). Reactive nonmalignant lymph node biopsies were collected at Centre Hospitalier Universitaire de Rennes. After mincing, tonsillar and lymph node mononuclear cells were isolated by Ficoll-density gradient centrifugation. BM aspirates were collected from adult patients undergoing thoracic surgery (Centre Hospitalier Universitaire de Rennes) and BM mononuclear cells were isolated by Ficoll density gradient centrifugation. Tonsils, lymph node biopsies, and BM aspirates were all collected after subject recruitment followed Institutional Review Board approval and written informed consent process according to the Declaration of Helsinki.

Cell cultures

In step one, B cell activation, all cultures were performed in IMDM (Invitrogen) and 10% FCS (Invitrogen), supplemented with 50 μg/ml human transferrin and 5 μg/ml human insulin (Sigma-Aldrich, St Louis, MO). Purified MBCs were cultured with IL-2 (20 U/ml), IL-10 (50 ng/ml), and IL-15 (10 ng/ml) in six-well culture plates (1.5×10^{5}/ml in 5 ml/well). Phosphorothioate CpG ODN 2006 (10 μg/ml; Sigma-Aldrich) (22), histidine-tagged recombinant human soluble CD40L (sCD40L; 50 ng/ml) and anti-polyhistidine mAb (5 μg/ml) (R&D Systems) were added at culture start. In step two, PB generation, at D4 culture, the cells were harvested, washed, and seeded at 2.5×10^{5}/ml with IL-2 (20 U/ml), IL-6 (50 ng/ml), IL-10 (50 ng/ml), and IL-15 (10 ng/ml). In step three, PC generation, at D7 culture, cells were washed and cultured at 5×10^{5}/ml with IL-6 (50 ng/ml), IL-15 (10 ng/ml), and IFN-α (500 U/ml) for 3 d.

Cell cycle analysis and immunophenotypic analysis

The percentage of cells in the S phase of the cell cycle was determined using propidium iodide, and data were analyzed with ModFit LT software (Verity Software House, Topsham, ME) (23). Cells were stained with combination of four to seven mAbs conjugated to different fluorochromes. Surface staining was performed prior to cell fixation and permeabilization. The Cytofix/Cytoperm kit (BD Biosciences) was used for intracellular staining of IgM, IgA, IgG, and Ki67 Ag, according to the manufacturer's recommendations. Flow cytometry analysis was performed with a FACSAria cytometer using FACSDiva 6.1 (Becton Dickinson, San Jose, CA) and with a Cyan ADP cytometer driven by Summit software (Beckman Coulter). For data analysis, CellQuest (Becton Dickinson), Summit, Kalusa (Beckman Coulter), and Infinicit 1.3 (Cytognos, Salamanca, Spain) softwares

were used. The fluorescence intensity of the cell populations was quantified using the stain index (SI) formula: (mean fluorescence intensity obtained from the given mAb minus mean fluorescence intensity obtained with a control mAb)/(2 × SD mean fluorescence intensity obtained with the same control mAb) (24). The extensive phenotypic study of tonsil cells was carried out using the multicolor flow cytometry methodology and Abs we previously reported in detail (25).

Analysis of Ig secretion

ELISPOT. D4 CD20$^-$CD38$^-$, D7 CD20$^-$CD38$^+$, and D10 CD20$^-$CD138$^+$ cells were purified using cytometry cell sorting and cultured for 18 h in ELISPOT plates (Millipore, Bedford, MA), which were precoated with goat anti-human IgM, IgA, or IgG polyclonal Abs (Caltag Laboratories, Birlingame, CA). After nine PBS washings, alkaline phosphatase-conjugated goat anti-human IgM, IgA, or IgG Abs (Tebu-Bio, Le Perray-en-Yvelines, France) were added for 6 h at 37°C. After three PBS washings, a mixture of NBT/5-bromo-4-chloro-3-indolyl phosphate substrate (Sigma-Aldrich) was added and reaction was stopped with distilled water. IgM-, IgA-, and IgG-secreting-cells were enumerated and immunospot size was assessed using the Biosys Bioreader 5000 apparatus (Biosys, Miami, FL).

ELISA. D4 CD20$^-$CD38$^-$, D7 CD20$^-$CD38$^+$, and D10 CD20$^-$CD138$^+$ cells were cytometry cell sorted, cultured for 24 h, and culture supernatants were harvested. IgM, IgA, and IgG secretions were assessed by ELISA using goat anti-human Igs for coating and secondary HRP-conjugated Abs specific for human γ-, α-, or μ-H chains, respectively (all from Jackson ImmunoResearch Laboratories, Newmarket, U.K.) as previously described (18).

Real-time RT-PCR analysis

Total RNA was extracted using the RNeasy kit (Qiagen, Valencia, CA) and reverse transcribed with a reverse transcription kit (Qiagen). The Assays-on-Demand primers and probes and the TaqMan Universal Master Mix were used according to the manufacturer's instructions (Applied Biosystems, Courtaboeuf, France). The primers used for assessing specific expression of spliced or unspliced forms of *XBP1* mRNA were from Applied Biosystems (Hs0329085 and Hs02856596 primers). Real-time RT-PCR was performed using the ABI Prism 7000 sequence detection system and normalized to β_2-microglobulin for each sample, and compared with the values obtained for a known positive control using the following equation: $100/2^{\Delta\Delta Ct}$, where $\Delta\Delta Ct = \Delta Ct$ unknown $- \Delta Ct$ positive control as described (26).

Microarray hybridization and bioinformatic analysis

RNA was extracted and hybridized to human genome U133 Plus 2.0 GeneChip microarrays, according to the manufacturer's instructions (Affymetrix, Santa Clara, CA). Gene expression data from D4 CD20^{high} CD38$^-$ cells, D4 CD20^{low}CD38$^-$ cells, and DCD20$^-$CD38$^-$ cells are deposited in the ArrayExpress public database (http://www.ebi.ac.uk/microarray-as/ae/, accession no. E-MEXP-3034). Gene expression data from D0 MBCs, D7 PBs, D10 PCs and purified BM PCs were from the ArrayExpress public database (http://www.ebi.ac.uk/microarray-as/ae/, accession number E-MEXP-2360). Gene expression data were analyzed with our bioinformatics platforms (RAGE, http://rage.montp.inserm.fr/) (27) and Amazonia (http://amazonia.transcriptome.eu/) (28). The clustering was performed and visualized with the Cluster and TreeView softwares (29). Gene differentially expressed between cell populations was determined with the significance analysis of microarray (SAM) statistical microarray analysis software (30).

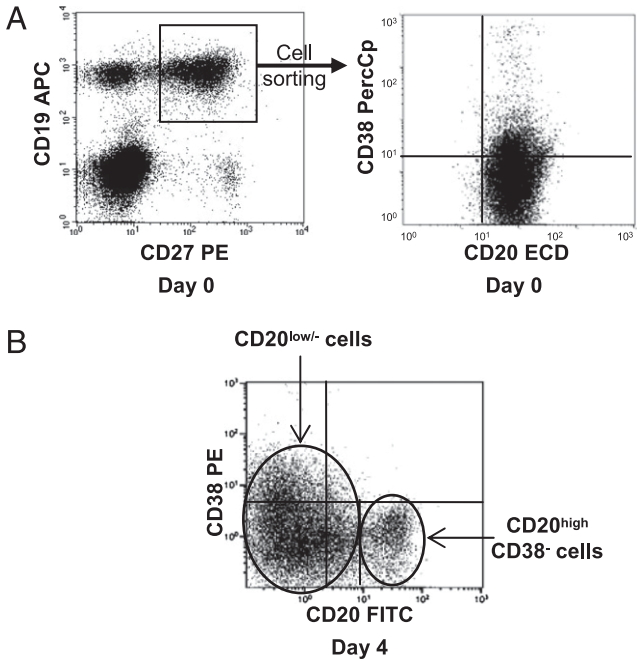

FIGURE 1. A 4-d activation of MBCs by sCD40L and CpG ODN yields two cell populations. MBCs were purified and cultured for 4 d using sCD40L and CpG ODN activation and IL-2 plus IL-10 plus IL-15 cytokines. At D4, the cell phenotype was assayed with fluorochrome-conjugated anti-CD20 and anti-CD38 mAbs, or isotype-matched control mAbs. Fluorescence was determined with a FACScan device. Results are those of 1 experiment representative of 17. *A*, Purification and phenotype of D0 starting MBCs. *B*, Phenotype of D4-activated cells. The vertical and horizontal lines in the second dot plot in *A* (*right panel*) and *B* correspond to the positive threshold defined with fluorochrome-conjugated isotype control mAbs. The second vertical half line in *B* defines the border between CD20^{high} and CD20$^{low/-}$ populations.

Statistical analysis

Statistical comparisons were made with the nonparametric Mann–Whitney *U* test and the unpaired or paired Student *t* test using SPSS software. A *p* value of ≤0.05 was considered as significant.

Table I. Expression of surface and cytoplasmic IgH isotypes by MBCs and D4 activated cells

	D0		D4							
	MBCs		CD20^{high}CD38$^-$		CD20^{low}CD38$^-$		CD20$^-$CD38$^-$		CD20$^-$CD38$^+$	
	%	SI	%	SI	%	SI	%	SI	%	SI
sIgM	43 ± 12	36 ± 8	65 ± 3	10 ± 1	65 ± 5	9 ± 3	31 ± 2^{a,b}	7 ± 2	30 ± 1^{a,b}	6 ± 1
cyIgM	45 ± 10	9 ± 2	60 ± 11	30 ± 8	44 ± 14^{a}	115 ± 41^{a}	18 ± 13^{a,b}	135 ± 71^{a}	21 ± 14^{a,b}	173 ± 78^{a}
sIgA	27 ± 6	25 ± 10	20 ± 5	11 ± 1	14 ± 2	17 ± 2	29 ± 5^{b}	17 ± 1^{a}	37 ± 5^{b}	16 ± 1^{a}
cyIgA	25 ± 6	48 ± 15	25 ± 5	37 ± 8	25 ± 9	154 ± 38^{a}	33 ± 10	172 ± 44^{a}	44 ± 12^{a,b}	209 ± 61^{a,b}
sIgG	26 ± 5	33 ± 3	9 ± 2	7 ± 3	15 ± 1^{a}	12 ± 4	28 ± 3^{a,b}	12 ± 5	27 ± 9	18 ± 9
cyIgG	27 ± 5	10 ± 4	20 ± 6	11 ± 4	29 ± 6^{a}	24 ± 7^{a}	41 ± 4^{a,b}	32 ± 10^{a,b}	33 ± 7^{a}	48 ± 13^{a,b}
Ki67	2 ± 1	NA	93 ± 1	24 ± 2	96 ± 1	54 ± 6^{a}	98 ± 0^{a}	60 ± 8^{a,b}	100 ± 0^{a}	77 ± 11
S-phase	0.5 ± 0	NA	25 ± 8	NA	56 ± 4^{a}	NA	56 ± 3^{a}	NA	46 ± 12^{a}	NA

MBCs were cultured as described in Fig. 1. Starting MBCs and D4-activated cells were labeled with fluorochrome-conjugated anti-CD20 and anti-CD38 mAbs, and with fluorochrome-conjugated anti-human IgM, IgA, IgG, and Ki67 mAbs or isotype-controlled mAbs before or after cell permeabilization or with propidium iodide. For each cell population, data are the mean percentage ± SD of positive cells and the mean staining indexes ± SD from three to five separate experiments.

[a] Mean expression is significantly different from that in D4 CD20^{high}CD38$^-$ cells.

[b] Mean expression is significantly different from that in D4 CD20^{low}CD38$^-$ cells.

NA, not applicable.

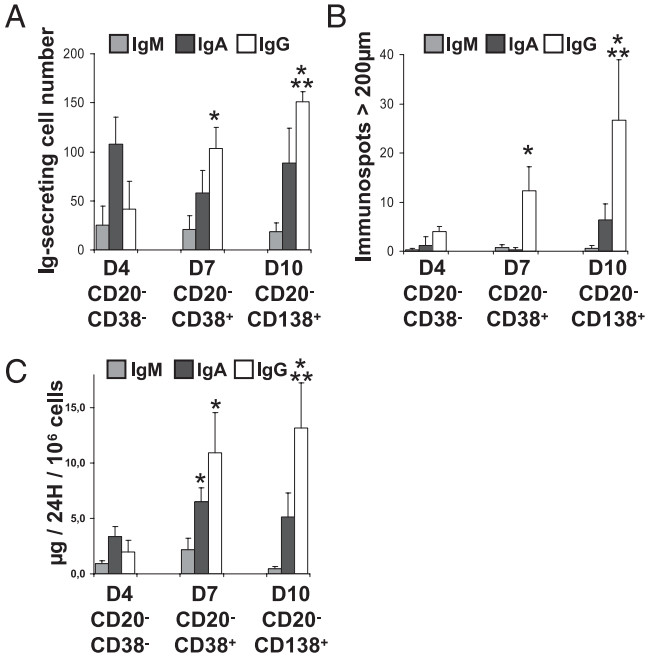

FIGURE 2. Ig secretion by D4 CD20$^-$CD38$^-$ cells, D7 PBs, and D10 PCs. D4 CD20$^-$CD38$^-$ cells, D7 CD20$^-$CD38$^+$ PBs, and D10 CD20$^-$CD138$^+$ PCs were flow cytometry cell sorted and cultured for 18 h in ELISPOT plates or cultured for 24 h and culture supernatants were harvested. The number of IgM-, IgA-, and IgG-secreting cells was assessed by ELISPOT. Results are (*A*) the mean number of IgM-, IgA-, and IgG-secreting cells, and (*B*) the mean number of immunospots with a size ≥200 µm determined in three separate experiments. *C*, IgM, IgA, and IgG secretions were assessed by ELISA and results are the mean Ig production in micrograms per day and per 10^6 cells determined in three separate experiments. *The mean is significantly different from that in D4 CD20$^-$CD38$^-$ cells ($p \leq 0.05$). **The mean is significantly different from that in D7 CD20$^-$CD38$^+$ PBs ($p \leq 0.05$).

Results

Activation of MBCs by sCD40L and CpG ODN yields two distinct cell populations

In the first step of differentiation of MBCs into PCs, two distinct cell populations could be identified in 17 separate experiments based on CD20 and CD38 expressions at the end of a 4-d activation by sCD40L and CpG ODN (step one). These two populations were CD20^{high}CD38$^-$ cells and CD20$^{low/-}$ cells comprising, respectively, 18 ± 7 and 82 ± 7% of D4 cells (Fig. 1*B*). The CD20 and CD38 FACS dot plot data suggest that the CD20$^{low/-}$ cell population may account for a continuous wave of differentiation of CD20^{low}CD38$^-$ cells (27 ± 7% of D4 cells) into CD20$^-$CD38$^+$ cells (17 ± 7% of D4 cells) passing through a transitional CD20$^-$CD38$^-$ stage (30 ± 10% of D4 cells) (Fig. 1*B*). To demonstrate this, we further investigated the characteristics of D4 CD20^{low}CD38$^-$, CD20$^-$CD38$^-$, and CD20$^-$CD38$^+$ subsets (referred to below as CD20$^{low/-}$ subsets).

Surface and cytoplasmic Ig expression and cell cycle in D4 CD20$^{low/-}$ cell subsets and in D4 CD20^{high}CD38$^-$ cells

The expression of surface (s) (sIgM, sIgA, sIgG) and cytoplasmic (cy) IgH isotypes (cyIgM, cyIgA, cyIgG) was looked for in the various D4 cell populations (Table I). Starting MBCs comprised the expected percentages of sIgM$^+$ (43 ± 12%), sIgA$^+$ (27 ± 6%), and sIgG$^+$ (26 ± 5%) cells (25, 31), and cell permeabilization did not increase the cytometry SI significantly, indicating that MBCs expressed mainly sIgs (Table I). In CD20^{low}CD38$^-$, CD20$^-$CD38$^-$, and CD20$^-$CD38$^+$ cells, the SI with anti-IgM or anti-IgA Abs increased 10- to 20-fold after cell permeabilization ($p < 0.05$), indicating that these cells were strongly involved in cyIg production (Table I, Supplemental Fig. 1). The increase in SI with the anti-IgG mAb was significant ($p < 0.05$) but less pronounced (2- to 4-fold) due to the use of allophycocyanin- and PerCP-Cy5.5-fluorochome–conjugated Abs, resulting in a lower SI as reported (32). Of note, CD20$^-$CD38$^-$ and CD20$^-$CD38$^+$ cells comprised increased IgG$^+$ and decreased IgM$^+$ cell numbers compared with CD20^{low}CD38$^-$ cells ($p < 0.05$; Table I). Conversely, D4 CD20^{high}CD38$^-$ cells expressed mainly sIgM$^+$ (65 ± 3%), and cell permeabilization slightly increased the SI for IgM and IgA ($p < 0.01$), unlike IgG. Additionally, CD20$^{low/-}$CD38$^-$ cells had a lower cytoplasmic Ig content compared with CD20$^-$CD38$^+$ cells as indicated by fluorescence intensity (Table I, Supplemental Fig. 1). The level of Ig secretion by the D4 CD20$^-$CD38$^-$ cell subset was further compared with that of in vitro-generated D7 PBs or D10 PCs using ELISPOT and ELISA. There were 8% IgG-secreting cells in D4 CD20$^-$CD38$^-$ cells,

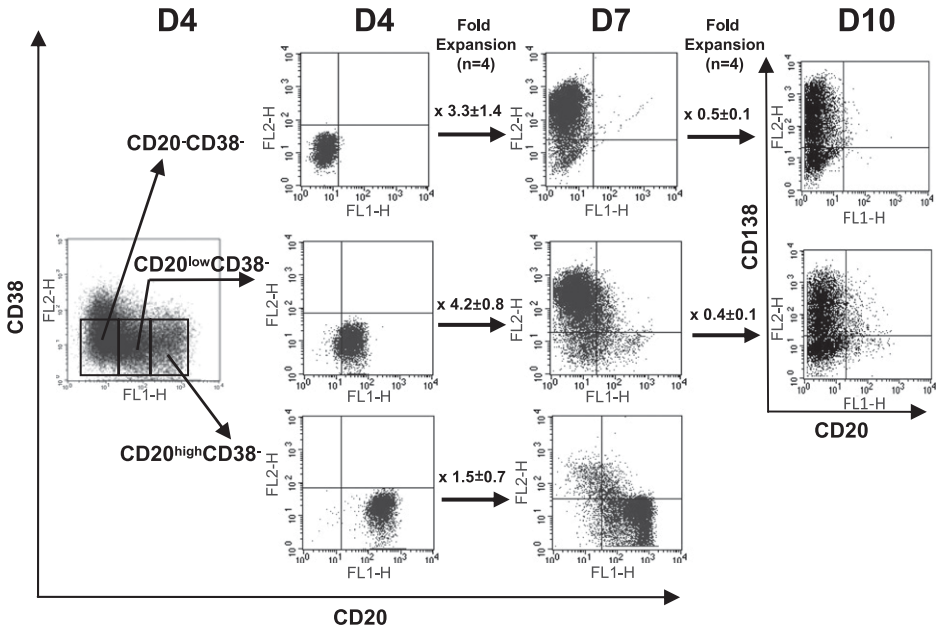

FIGURE 3. Plasmablast and plasma cell differentiation potential of D4 CD20$^{low/-}$CD38$^-$ prePBs and of D4 CD20^{high}CD38$^-$ cells. Purified MBCs were cultured for 4 d using sCD40L and CpG ODN activation and IL-2 plus IL-10 plus IL-15 cytokines. At D4, CD20^{high}CD38$^-$, CD20^{low}CD38$^-$, and CD20$^-$CD38$^-$ cells were FACS sorted and cultured for 3 d with PB culture conditions (IL-2 plus IL-6 plus IL-10 plus IL-15). D7 cells were washed and cultured for an additional 3 d with plasma cell culture conditions (IL-6 plus IL-15 plus IFN-α). At each culture step, the cell phenotype was assayed with fluorochrome-conjugated anti-CD20, anti-CD38, and anti-CD138 mAbs, or with isotype-matched control mAbs. Fluorescence was determined with a FACScan device. Results are those of one experiment representative of four, and the fold expansions are the mean values ± SD of those in four experiments.

that is, 2.5- and 3.7-fold less than in D7 PBs or D10 PCs ($p < 0.02$; Fig. 2*A*), and with a 3- to 7-fold smaller immunospot size (≥200 μm; Fig. 2*B*). The number of IgA-secreting cells in D4 CD20$^-$CD38$^-$ cells was not significantly different from those in D7 PBs or D10 PCs (Fig. 2*A*). There were 3–5% IgM-secreting cells in the D4 CD20$^-$CD38$^-$ cell subset as in D7 PBs and D10 PCs (Fig. 2*A*), with no difference in IgM immunospot size. The measurement of Ig production in culture supernatants confirmed ELISPOT data. D4 CD20$^-$CD38$^-$ cells secreted 5- to 7-fold less IgG, 1.5- to 2-fold less IgA, and similar IgM levels than did D7 PBs or D10 PCs (Fig. 2*C*).

Cell cycling was looked for with anti-Ki67 and propidium iodide staining (Table I). Starting MBCs were quiescent and all D4 cell populations were cycling with 93–100% Ki67$^+$ cells. CD20^{low} CD38$^-$, CD20$^-$CD38$^-$, and CD20$^-$CD38$^+$ cells had a higher proportion of cells in the S phase (46–56%) than did CD20^{high} CD38$^-$ cells (25%, $p < 0.05$).

These results indicate that the D4 CD20$^{low/-}$ cell population comprised mostly CD20$^{low/-}$CD38$^-$ cells that expressed cyIgs and secreted Igs, but at a weaker level than D7 PBs and D10 PCs. Given the Ig secretion, the lack of CD38 and the lack or weak expression of CD20 B cell marker, these CD20$^{low/-}$CD38$^-$ cells are termed prePBs in the following.

D4 CD20$^{low/-}$CD38$^-$ prePBs generate CD20$^-$CD38^{high} PBs and then CD138$^+$ plasma cells, unlike D4 CD20^{high}CD38$^-$ cells

The PC differentiation potential of D4 CD20$^{low/-}$CD38$^-$ prePBs was assayed culturing these cells for three additional days in PB step two culture conditions (Fig. 3). CD20$^{low/-}$CD38$^-$ cells were sorted into CD20^{low}CD38$^-$ and CD20$^-$CD38$^-$ cells to evaluate whether these two populations had a similar differentiation potential and thus could actually correspond to a unique cell subset. This was the case since a vast majority of both D4 CD20^{low} CD38$^-$ and D4 CD20$^-$CD38$^-$ cells differentiated into D7 CD20$^-$ CD38^{high} PBs in four separate experiments (73 ± 15 and 87 ± 7%, respectively) in association with a 4.2- or 3.3-fold cell expansion, respectively (Fig. 3). When further put into step three plasma cell culture conditions for 3 d (D7 to D10), the sorted CD20^{low}CD38$^-$ or CD20$^-$CD38$^-$ cells generated CD20$^-$ CD38^{high}CD138$^+$ PCs (51 ± 7 and 72 ± 5%, respectively; $n = 4$; Fig. 3). Conversely, D4 CD20^{high}CD38$^-$ cells gave rise to few CD38$^+$CD20$^-$ cells (23 ± 13%, $n = 4$) in step two culture conditions, and did not survive when further put in step three plasma cell culture conditions (Fig. 3). Thus, these in vitro differentiation data reveal the presence of only two populations of CD38$^-$ cells at D4 of culture: first, actively cell cycling CD20$^{low/-}$CD38$^-$ prePBs that efficiently differentiated into CD20$^-$CD38^{high} PBs and then CD20$^-$CD38^{high}CD138$^+$ PCs; and second, CD20^{high}CD38$^-$ cells that poorly differentiated and survived into PB and then PC culture conditions.

Molecular characterization of D4 CD20$^{low/-}$CD38$^-$ prePBs

The gene expression of sorted D4 CD20^{high}CD38$^-$, CD20^{low} CD38$^-$, and CD20$^-$CD38$^-$ cells obtained from MBCs from five healthy donors was profiled using Affymetrix U133 Plus 2.0 microarrays. An unsupervised hierarchical clustering using the 5000 probe sets with the highest SD made it possible to cluster CD20^{high}CD38$^-$ cells together and CD20$^{low/-}$CD38$^-$ prePBs in another cluster (Fig. 4*A*). Of note, inside the CD20$^{low/-}$CD38$^-$ cluster, CD20^{low}CD38$^-$ and CD20$^-$CD38$^-$ cells originating from a same donor were grouped together for three of the five donors, emphasizing that these two cell subsets constituted a homogeneous population (Fig. 4*A*). This was confirmed using paired supervised analysis, since only 23 probe sets of 5000 were differentially expressed between CD20^{low}CD38$^-$ and CD20$^-$ CD38$^-$ cells (ratio ≥ 2, 1000 permutations, false discovery rate 0%; results not shown). Comparing CD20$^-$CD38$^-$ and CD20^{high} CD38$^-$ cells, 695 probe sets fully discriminated the two cell populations using paired SAM supervised analysis (ratio ≥ 2, 1000 permutations, 0% false discovery rate) (Fig. 4*B*). They encoded for 495 unique genes, of which 267 were upregulated in CD20^{high}CD38$^-$ cells and 228 in CD20$^-$CD38$^-$ cells. Table II shows the top 50 genes that were upregulated in each of the two cell populations, and the 495 unique genes are shown in Supplemental Table I. CD20$^-$CD38$^-$ prePBs highly expressed *Ig* genes in agreement with their increased cytoplasmic Ig expression, *IL-6R*, *BCMA* (*TNFRSF17*), and *CD59* that are PC markers.

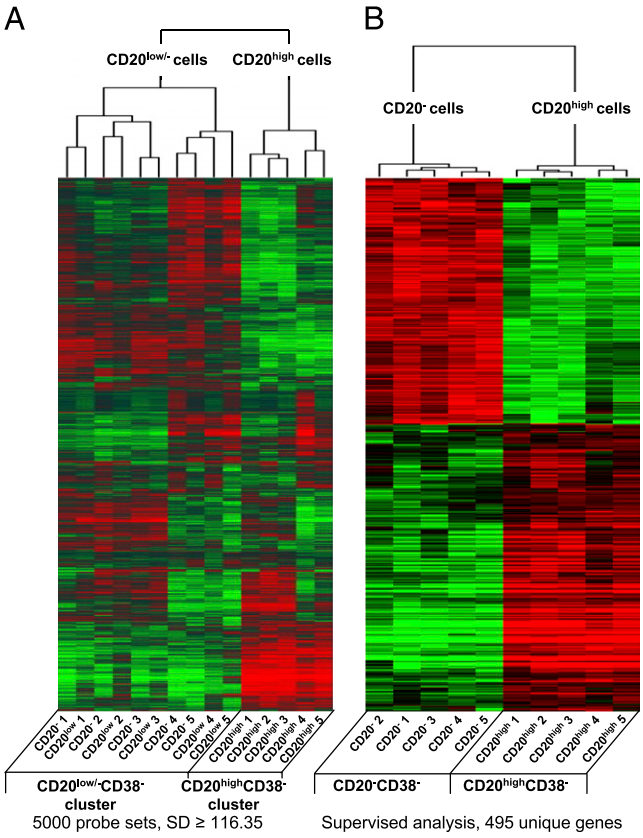

FIGURE 4. Unsupervised and supervised clustering of gene expression profiles of purified D4 CD20^{low}CD38$^-$ and CD20$^-$CD38$^-$ prePBs and of D4 CD20^{high}CD38$^-$ B cells. MBCs from five donors (numbered 1–5) were cultured for 4 d with sCD40L, CpG ODN, and IL-2 plus IL-10 plus IL-15 cytokines. D4 CD20^{high}CD38$^-$, CD20^{low}CD38$^-$, and CD20$^-$CD38$^-$ cells were FACS sorted and their gene expression profiling was assayed with Affymetrix U133 Plus 2.0 microarrays. *A*, An unsupervised hierarchical clustering was run with the 5000 probe sets with the highest SD (log transform, center genes and arrays, uncentered correlation, and average linkage). The dendogram shows that CD20^{high}CD38$^-$ samples and CD20$^{low/-}$CD38$^-$ samples are grouped in two separate clades ($r = 0.44$). In the CD20$^{low/-}$CD38$^-$ clade, CD20^{low}CD38$^-$ and CD20$^-$CD38$^-$ cells originating from the same donor cluster together for three of five donors, indicating that these two populations are close. *B*, The probe sets differentially expressed between D4 CD20^{high}CD38$^-$ and CD20$^-$CD38$^-$ cells were determined with a SAM supervised analysis for pairs (Wilcoxon statistic, 2-fold ratio, 0% false discovery rate), identifying 495 unique genes. When a gene was assayed by several probe sets, the probe set with the highest variance was used. An unsupervised hierarchical clustering was run on this 495 unique gene list. The normalized expression value for each gene is indicated by a color, with red representing high expression and green representing low expression.

Table II. $CD20^{-}CD38^{-}$ and $CD20^{high}CD38^{-}$ top 50 overexpressed genes

$CD20^{-}CD38^{-}$ Genes				$CD20^{high}CD38^{-}$ Genes			
Gene ID	Gene Name	Fold Change	Score (d)	Gene ID	Gene Name	Fold Change	Score (d)
205945_at	IL6R	18.41	4.44	232739_at	SPIB	0.01	−2.68
235275_at	BMP8B	15.78	3.16	224402_s_at	FCRL4	0.01	−5.48
203914_x_at	HPGD	14.66	2.65	226818_at	MPEG1	0.01	−2.91
204798_at	MYB	10.80	7.09	235385_at	MARCH-I	0.01	−3.98
222392_x_at	PERP	9.68	3.86	223343_at	MS4A7	0.01	−4.75
203373_at	SOCS2	9.35	5.81	204959_at	MNDA	0.01	−4.11
221790_s_at	LDLRAP1	8.87	3.35	266_s_at	CD24	0.01	−4.43
201324_at	EMP1	8.67	3.79	204249_s_at	LMO2	0.01	−14.17
206641_at	TNFRSF17/BCMA	6.86	5.37	219517_at	ELL3	0.01	−8.97
201243_s_at	ATP1B1	6.67	2.67	228055_at	NAPSB	0.02	−9.02
233500_x_at	CLEC2D	6.45	3.15	217418_x_at	MS4A1/CD20	0.02	−14.56
201678_s_at	DC12	6.22	3.95	205987_at	CD1C	0.03	−7.57
39248_at	AQP3	6.08	9.19	231093_at	FCRH3	0.03	−5.07
200983_x_at	CD59	5.32	2.49	228153_at	IBRDC2	0.03	−2.97
206729_at	TNFRSF8/CD30	5.25	2.61	207339_s_at	LTB	0.04	−4.80
204254_s_at	VDR	5.20	3.22	208018_s_at	HCK	0.05	−5.33
221760_at	MAN1A1	5.04	12.00	208820_at	PTK2	0.05	−2.79
220306_at	FAM46C	5.01	3.56	210279_at	GPR18	0.05	−5.82
209457_at	DUSP5	4.90	3.08	238009_at	SOX5	0.06	−5.17
205885_s_at	ITGA4	4.73	2.58	213293_s_at	TRIM22	0.06	−7.82
203397_s_at	GALNT3	4.61	4.02	219014_at	PLAC8	0.06	−4.11
206632_s_at	APOBEC3B	4.61	4.79	228617_at	BIRC4BP	0.06	−2.80
217127_at	CTH	4.59	5.13	206126_at	BLR1	0.07	−4.05
1554242_a_at	COCH	4.59	3.11	204581_at	CD22 /// MAG	0.07	−4.39
202241_at	TRIB1	4.58	9.99	216080_s_at	FADS3	0.07	−3.79
224802_at	NDFIP2	4.52	2.81	221234_s_at	BACH2	0.07	−4.31
209921_at	SLC7A11	4.52	3.40	213111_at	PIP5K3	0.07	−11.02
201397_at	PHGDH	4.52	2.93	225123_at	SESN3	0.08	−4.27
203474_at	IQGAP2	4.44	5.23	215933_s_at	HHEX	0.08	−5.42
200951_s_at	CCND2	4.13	8.53	205128_x_at	PTGS1	0.08	−2.75
203066_at	GALNAC4S-6ST	4.09	3.15	218032_at	SNN	0.09	−2.97
218018_at	PDXK	4.08	2.66	205922_at	VNN2	0.09	−2.89
219118_at	FKBP11	4.03	2.99	204440_at	CD83	0.09	−7.96
204900_x_at	SAP30	3.97	4.52	203186_s_at	S100A4	0.09	−3.34
202558_s_at	STCH	3.97	4.01	221011_s_at	LBH	0.10	−4.42
224851_at	CDK6	3.96	3.14	204994_at	MX2	0.10	−3.19
211464_x_at	CASP6	3.92	2.59	206983_at	CCR6	0.10	−4.88
200628_s_at	WARS	3.87	4.70	200696_s_at	GSN	0.10	−2.79
217824_at	UBE2J1	3.85	5.86	219836_at	ZBED2	0.10	−7.02
225512_at	ZBTB38	3.78	7.76	1559263_s_at	ZC3H12D	0.10	−6.97
202468_s_at	CTNNAL1	3.67	3.44	227458_at	PDCD1LG1	0.10	−5.18
218073_s_at	TMEM48	3.60	3.70	38521_at	MAG	0.10	−7.58
228964_at	PRDM1	3.57	4.17	230110_at	MCOLN2	0.11	−5.00
209695_at	PTP4A3	3.55	3.79	223751_x_at	TLR10	0.11	−5.58
203971_at	SLC31A1	3.53	3.51	229937_x_at	LILRB1	0.11	−4.08
216044_x_at	FAM69A	3.50	3.58	226748_at	LYSMD2	0.11	−3.05
225520_at	MTHFD1L	3.49	9.94	203233_at	IL4R	0.11	−3.57
222385_x_at	SEC61A1	3.47	2.86	224499_s_at	AICDA	0.12	−5.11
201206_s_at	RRBP1	3.44	3.22	215127_s_at	RBMS1	0.12	−3.48
226771_at	ATP8B2	3.41	4.57	1552807_a_at	SIGLEC10	0.12	−2.99

Additionally, they expressed *CD30* (*TNFRSF8*) and *EMP1* (Table II, Supplemental Table I). Conversely, $CD20^{high}CD38^{-}$ cells highly expressed genes for B cell Ags, that is, *CD19*, *CD20* (*MS4A1*), *CD22*, and *CD24* (Table II, Supplemental Table I).

Phenotype of D4 $CD20^{low/-}CD38^{-}$ cells

FACS analysis confirmed Affymetrix data. D4 $CD20^{low/-}CD38^{-}$ cells expressed higher levels of IL-6R, CD30, CCR10, and CD43 than did D4 $CD20^{high}CD38^{-}$ cells (Fig. 5, Table III). Conversely, D4 $CD20^{high}CD38^{-}$ cells expressed higher levels of CD24, CD19, CD45, CXCR5, and CD27 than did D4 $CD20^{low/-}CD38^{-}$ cells (Fig. 5, Table III). Of note, CD27 dramatically increased again when D4 $CD20^{low/-}CD38^{-}$ cells differentiated into D7 PBs and D10 PCs as documented previously (31). D4 $CD20^{low}CD38^{-}$ cells had a phenotype close to that of $CD20^{-}CD38^{-}$ cells, but with a significantly weaker expression of prePB and PB markers (CD30, IL-6R, and CD43), in agreement with gene expression data.

B to plasma cell atlas

An open access "B to Plasma Cell Atlas" was developed allowing interrogating gene expression of D4 $CD20^{low/-}CD38^{-}$ prePBs and $CD20^{high}CD38^{-}$ B cells together with those of MBCs, PBs, early PCs, and BMPCs (31). For convenient atlas use, D4 $CD20^{low}CD38^{-}$ cells, D4 $CD20^{-}CD38^{-}$ cells, and D4 $CD20^{high}CD38^{-}$ cells are termed $CD20^{low}$ prePBs, $CD20^{-}$ prePBs, and $CD20^{high}$ B cells. This open access atlas can be visualized on our Amazonia Web site (http://amazonia.transcriptome.eu/index.php?zone=PlasmaCell). Fig. 6*A* displays the expression of genes coding for transcription factors controlling B cell or PC fates, and Fig. 6*B* displays the validation of these gene expressions by real-time RT-PCR. $CD20^{low/-}$ prePBs weakly expressed *PAX5* B cell transcription

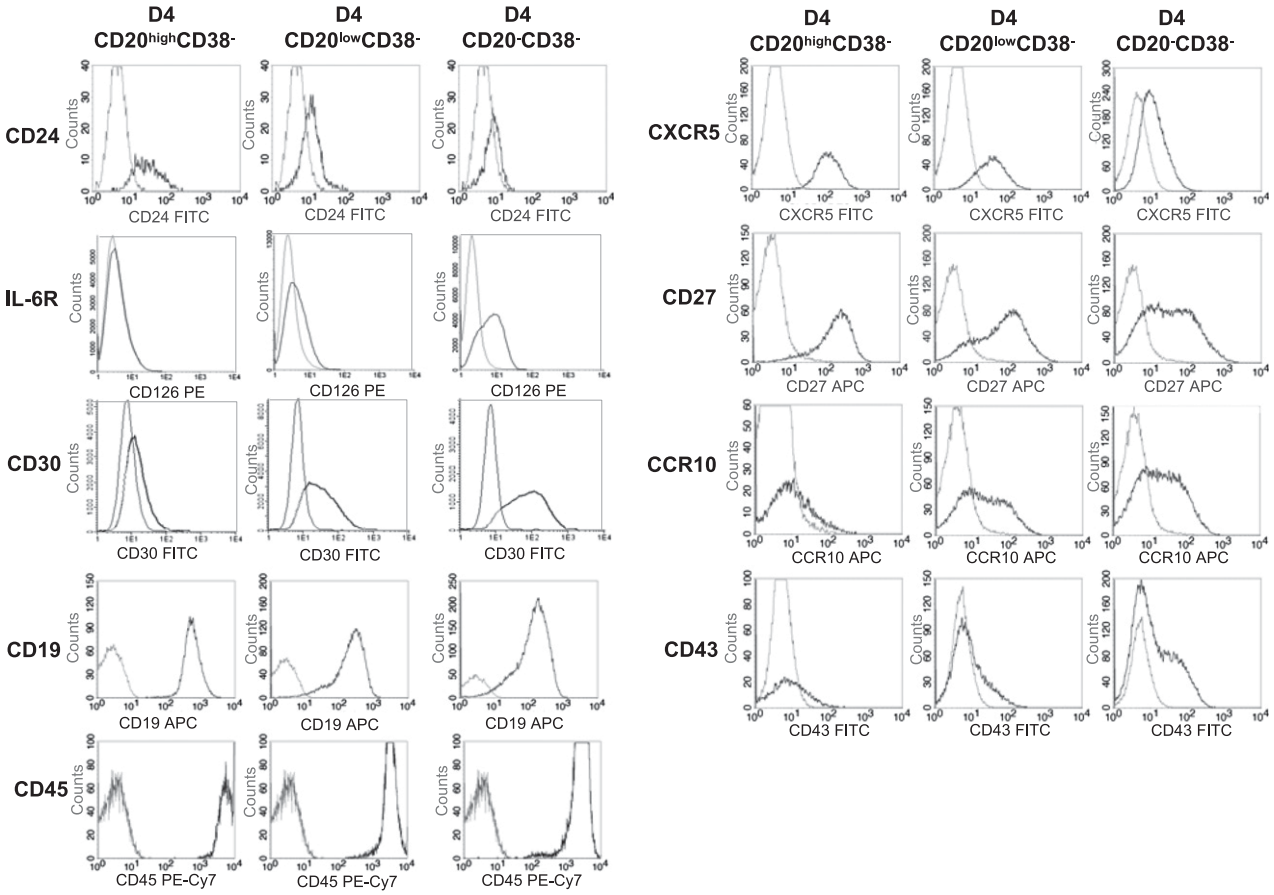

FIGURE 5. Phenotype and expression of homing molecules of D4 CD20^{low}CD38^{-} and D4 CD20^{-}CD38^{-} prePBs and of D4 CD20^{high}CD38^{-} cells. MBCs were cultured as described in Fig. 1. Cells were stained for CD20 and CD38 and the cell phenotype was analyzed by gating on D4 CD20^{high}CD38^{-} cells, D4 CD20^{low}CD38^{-} cells, and D4 CD20^{-}CD38^{-} cells. Black histograms show FACS labeling with anti-CD24, IL-6R, CD30, CD19, CD45, CXCR5, CD27, CCR10, and CD43. Gray histograms display the corresponding negative control mAbs. Data from one experiment representative of three to five are shown.

factor and PAX5 target genes (*IRF8*, *BACH2, EBF1, SPIB*) (Fig. 6*A*, 6*B*) as well as *BCL6* gene (Fig. 6*B*). CD20$^{low/-}$ prePBs expressed PC transcription factor genes *PRDM1* and *XBP1* at a weaker level than PBs or early PCs (Fig. 6*A*). Because *XBP1* mRNA has to be spliced by IRE1 endonuclease to encode for an active XBP1 protein (33), spliced *XBP1* (*XBP1*s) and unspliced (*XBP1*u) mRNAs were quantified. D4 prePBs expressed high levels of *XBP1* mRNA, mainly *XBP1*u mRNA. The *XBP1*s/*XBP1*u mRNA ratio was 0.3 in prePBs, and this ratio was increased 3.5- to 5-fold in D7 PBs and D10 PCs that expressed *XBP1*s mRNA mainly (Fig. 6*C*). The expression of genes coding for B cell and PC surface markers or homing molecules are displayed in Supplemental Figs. 2 and 3. Affymetrix data are in agreement with the phenotype of prePBs reported above: lack of B cell Ags and of CD38. Of interest, prePBs specifically expressed *CD30* and *EMP1* genes, unlike B cells, PBs, early PCs, or BMPCs. PrePB genes were significantly higher and B cell genes lower in CD20^{-} prePBs than in CD20^{low} prePBs.

Table III. Expression of membrane markers by MBCs and D4 activated cells

	D0 MBCs		D4 CD20^{high}CD38^{-}		D4 CD20^{low}CD38^{-}		D4 CD20^{-}CD38^{-}	
Membrane Markers	%	SI	%	SI	%	SI	%	SI
CD24	88 ± 4	82 ± 15	68 ± 21	25 ± 41	31 ± 36[a]	5 ± 7[a]	5 ± 4[a,b]	0.7 ± 0.5[a,b]
IL-6R	0.6 ± 0.9	0 ± 0	0 ± 0	0 ± 0	26 ± 8[a]	0.5 ± 0.1[a]	60 ± 9[a,b]	1.3 ± 0.4[a,b]
CD30	0 ± 0	0 ± 0	30 ± 5	0.9 ± 0.4	70 ± 7[a]	7 ± 0[a]	87 ± 4[a]	17 ± 2[a,b]
CD19	100 ± 0	45 ± 13	100 ± 0	225 ± 73	92 ± 3[a]	64 ± 12[a]	89 ± 4[a,b]	41 ± 6[a,b]
CD45	100 ± 0	718 ± 51	100 ± 0	782 ± 497	100 ± 0	425 ± 245[a]	100 ± 0	353 ± 193[a,b]
CXCR5	97 ± 2	7 ± 1	98 ± 0	20 ± 4	61 ± 11[a]	6 ± 2[a]	15 ± 2[a,b]	1.5 ± 0.4[a]
CCR10	1.3 ± 0.5	0 ± 0	21 ± 9	1.7 ± 1.1	42 ± 6[a]	4.2 ± 1.6	41 ± 5	3.9 ± 1.4
CD43	9 ± 1	2.0 ± 0.4	18 ± 3	1.8 ± 0.6	14 ± 3	1.3 ± 0.5	31 ± 6[b]	3.6 ± 1.5
CD27	100 ± 0	9 ± 1	84 ± 7	31 ± 9	66 ± 10[a]	20 ± 7[a]	42 ± 12[a,b]	11 ± 4[a,b]

MBCs were cultured as described in Fig. 1. Starting MBCs, D4-activated cells were labeled with fluorochrome-conjugated anti-CD20 and anti-CD38 mAbs and with indicated fluorochrome-conjugated mAbs or isotype-controlled mAbs. For each cell population, data are the mean percentage ± SD of positive cells and the mean staining indexes ± SD from three to five separate experiments.

[a]Mean expression is significantly different from that in D4 CD20^{high}CD38^{-} cells.

[b]Mean expression is significantly different from that in D4 CD20^{low}CD38^{-} cells.

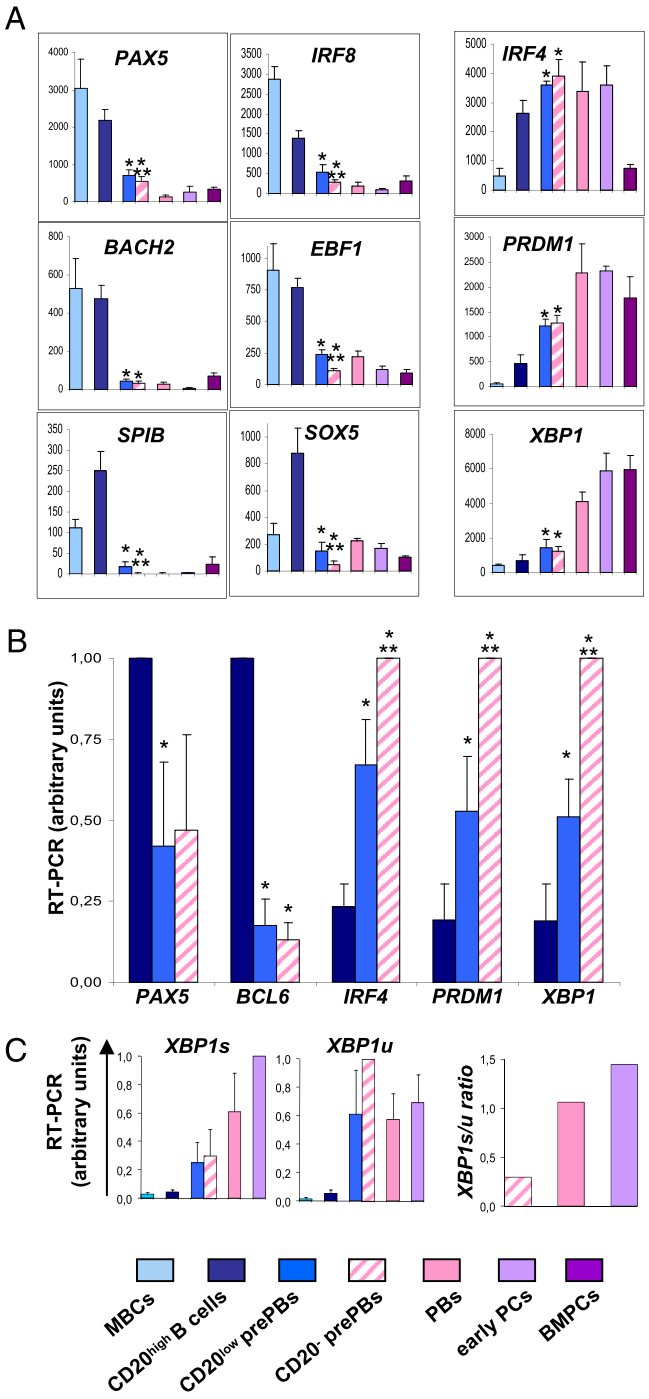

FIGURE 6. Expression of genes coding for transcription factors governing B cell to PC differentiation. The gene expression of the 54613 Affymetrix probe sets in various B cell and plasma cell populations can be visualized using the Amazonia Web site (http://amazonia.transcriptome.eu/index.php?zone=PlasmaCell): MBCs (clear blue), D4 CD20^{high}CD38^{-} cells termed CD20^{high} B cells (dark blue), D4 CD20^{low}CD38^{-} cells termed CD20^{low} prePBs (blue), D4 CD20^{-}CD38^{-} cells termed CD20^{-} prePBs (dashed pink), PBs (pink), early PCs (clear violet), and BMPCs (dark violet) gene expression profiling of prePBs, PBs, early PCs, and BMPCs were available from ArrayExpress public database (http://www.ebi.ac.uk/microarray-as/ae/, accession nos. E-MEXP-3034 and E-MEXP-2360). *A*, Affymetrix signals of expression of genes coding for transcription factors controlling B cell and PC cell fate. Data are the mean value ± SD of gene expression determined in five separate experiments. *B*, Validation of gene expression of *PAX5*, *BCL6*, *IRF4*, *PRDM1*, and *XBP1* by real-time RT-PCR. *C*, Quantification of *XBP1*s and *XBP1*u mRNA by real-time RT-PCR and *XBP1*s/*XBP1*u ratio in CD20^{-} prePBs, PBs, and PCs. The mRNA level in the different cell populations was compared assigning the arbitrary value 1 to the maximal expression. Data are the mean value ± SD of mRNA level or ratio determined in three separate experiments. *The mean expression is significantly different from that in CD20^{high} B cells ($p \leq 0.05$). **The mean expression is significantly different from that in CD20^{low} prePBs ($p \leq 0.05$).

In vivo detection of CD20$^{low/-}$CD38^{-} prePBs

The presence of prePBs, defined as CD19^{+}CD20$^{low/-}$CD38^{-} CD138^{-} cells, was looked for in human tonsils and reactive lymph nodes. Fig. 7*A* shows that gating consecutively on CD19^{+} cells and then CD20^{-} cells made it possible to detect a minor population of CD38^{-} and CD138^{-} cells in seven of seven tonsil samples and in seven of nine lymph node samples. This CD19^{+} CD20$^{low/-}$CD38^{-}CD138^{-} population accounted for 0.06 ± 0.02 (range, 0.02–0.08%) and 0.05 ± 0.03% (range, 0.02–0.09%) of CD19^{+} cells in tonsil and positive lymph node samples, respectively. CD19^{+}CD20$^{low/-}$CD38^{-}CD138^{-} cells could not be detected in BM (five samples) and peripheral blood (five samples, data not shown). Looking for cytoplasmic Ig expression, approximately two thirds of these CD19^{+}CD20$^{low/-}$CD38^{-}CD138^{-} cells expressed high levels of Ig L chains after cell permeabilization (Fig. 7*B*). The other third expressed one log weaker levels of Ig L chain after cell permeabilization and we previously showed these cells are B cells that express surface Ig L chains (25). Fig. 7*C* shows that a large part of in vivo CD19^{+}CD20$^{low/-}$CD38^{-} CD138^{-} cells also expressed IL-6R, unlike CD19^{+}CD20^{+} cells. Thus, 45 ± 5% of CD19^{+}CD20$^{low/-}$CD38^{-}CD138^{-} cells are IL-6R^{+} in tonsils (range, 36–51%) and 36 ± 14% are IL-6R^{+} in lymph nodes (range, 18–57%).

Discussion

Owing to the rarity of plasma cells and their anatomic location, the early stages of differentiation of B cells into plasma cells are not fully elucidated, in particular in humans. Using an in vitro model mimicking T cell help, we report a transitional prePB stage in the differentiation of human memory B lymphocytes into PBs, and then plasma cells. These prePBs are characterized by the loss of B cell markers, except CD19, a decrease in CD27, the lack of CD38, and by the secretion of Igs at a lower level than CD38^{+} PBs or CD138^{+} plasma cells. Their prePB status is evidenced by their ability to fully differentiate into PBs that highly express CD38 within 3 d (CD19^{+}CD20^{-}CD38^{high} cells) and then plasma cells that express CD138 within additional 3 d (CD19^{+}CD20^{-}CD38^{high} CD138^{+} cells). Human CD38$^{-/low}$ Ig-secreting cells were already reported but with challenging results regarding their behavior and phenotype. With a model of MBC activation by CD40L and cytokines close to the current one, Tangye et al. (20) reported that CD38^{-} B cells poorly survived upon removal of CD40L activation and were thought to be precursors of short-living plasma cells. In the current study, sorted CD20$^{low/-}$CD38^{-} prePBs efficiently differentiated into PBs and then plasma cells. An explanation could be the use of whole CD38^{-} B cells in the study by Tangye et al. comprising activated B cells (here CD20^{high}CD38^{-} cells) and prePBs, avoiding an efficient differentiation of prePBs. In a following study published by Avery et al. (21) using a similar in vitro model, precursors of Ig-secreting cells were shown to be mainly CD27^{high} cells, independently of CD38 expression, and CD27^{low} cells had a reduced cell cycling. These data also do not fit with the current ones since prePBs have a reduced CD27 gene and protein expression compared with MBCs, PBs, or plasma cells. Additionally, the CD27^{low} prePBs were highly proliferating with

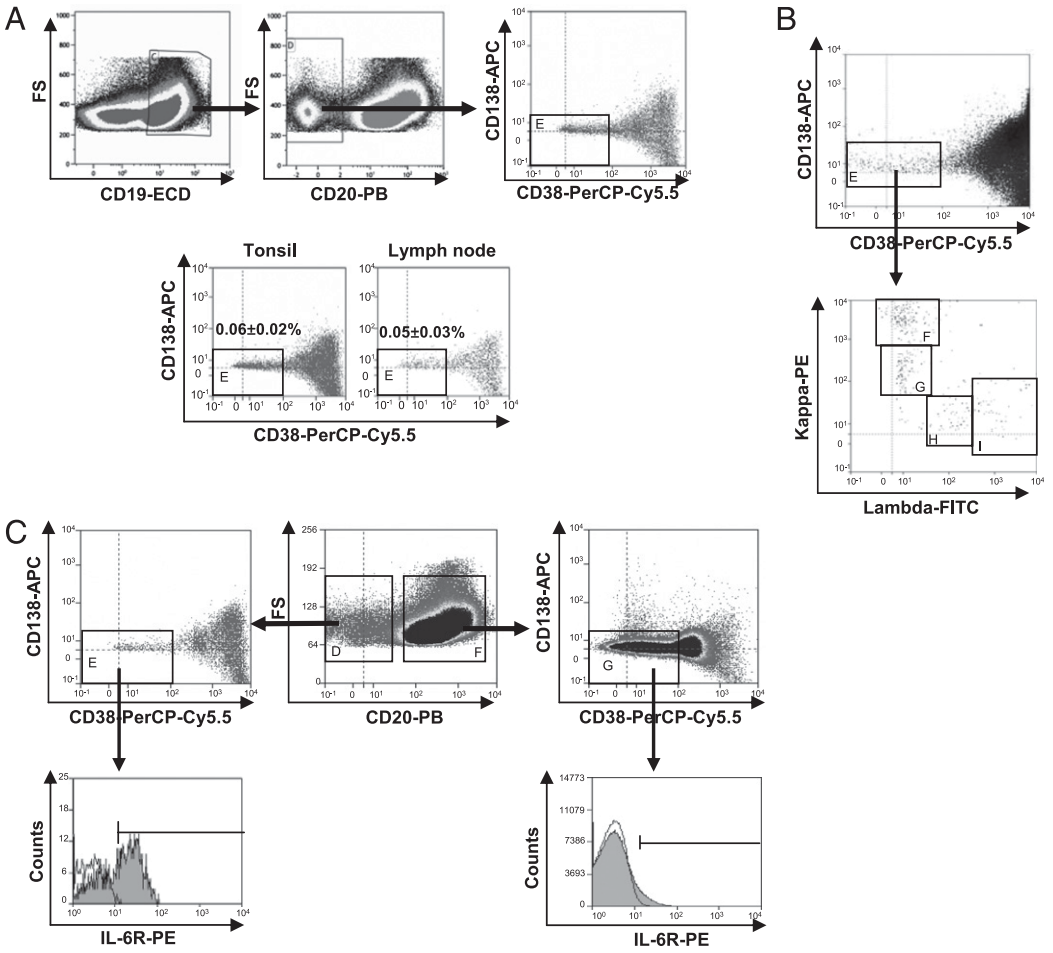

FIGURE 7. Detection of $CD20^{low/-}CD38^{-}IL\text{-}6R^{+}$ prePBs in human lymphoid tissues. Mononuclear cells isolated from tonsils (seven donors) and lymph nodes (nine donors) were stained for CD19, CD20, CD38, CD138, and IL-6R. *A*, A consecutive gating strategy on $CD19^{+}$ and then $CD20^{-}$ cells made it possible to identify $CD19^{+}CD20^{low/-}CD38^{-}CD138^{-}$ prePBs in lymphoid tissue samples. Numbers in the panels are the mean percentages ± SD of prePBs in $CD19^{+}$ cells in seven tonsils or nine lymph nodes. *B*, Cytoplasmic and membrane Ig L chain expression by $CD19^{+}CD20^{low/-}CD38^{-}CD138^{-}$ prePBs. A high expression of κ (F) and λ (I) L chains corresponded to cytoplasmic L chains, and an intermediate expression to membrane L chains. Data are from one representative experiment of two separate experiments. *C*, $CD19^{+}CD20^{low/-}CD38^{-}CD138^{-}$ prePBs IL-6R expression compared with $CD19^{+}CD20^{+}$ B cells. The bold histograms represent labeling with anti–IL-6R mAb and the light ones, with the control mAb. Data are from one representative experiment using tonsil cells.

50% of cells in the S phase. A possible explanation for these differences is that we used CpG ODN and CD40L stimulation of memory B cells, whereas Tangye et al. used CD40L stimulation only. CpG ODN is known to promote B cell differentiation activating TLRs. Thus, either CpG ODN can downregulate CD27 expression on prePBs that further differentiate into PBs, or the differentiation of $CD27^{low}$ prePBs may require both CD40L and TLR activation. Arce et al. (19) identified $CD38^{low/-}$ Ig-secreting cells in tonsils. These $CD38^{low/-}$ Ig-secreting cells were shown to weakly express CD27, in agreement with our current data. These cells were suggested to be precursors of $CD38^{high}$ Ig-secreting cells because they were detected earlier in culture of tetanus toxoid-activated B cells. However, this was not proven formally using cell sorting and culturing these $CD38^{low/-}$ cells.

The relevance of this transitional $CD19^{+}CD20^{-}CD38^{-}$ prePB stage is highlighted by the peaked expression of CD30 gene and protein. Memory B cells, PBs, early plasma cells, and BM plasma cells do not express CD30. CD30 is a TNFR family member that is expressed on activated T cells, EBV-infected B cells, some large diffuse lymphoma, Reed–Sternberg cells, and anaplastic large cell lymphoma. As CD30 is an activation molecule, we looked for a modulation of prePB proliferation or differentiation using CD30 activation by histidine-bound CD30L and anti-histidine Abs. No modulation was found in our culture conditions (data not shown).

The loss of CD20 and most B cell markers in prePBs could be likely explained by the decrease in PAX5 that controls expression of B cell genes (34–36). *PAX5* gene expression decrease in prePBs is associated with an upregulation of expression of *IRF4* and *PRDM1* genes and downregulation of *BCL6*. Thus, the usual crossregulation of B and plasma cell transcription factors should occur in prePBs: NF-κB induces upregulation of IRF4 that associates with STAT3 to trigger *PRDM1* gene activation and induces downregulation of *BCL6* gene expression, an inhibitor of *PRDM1* gene activation. The resulting expression of *PRDM1* gene product, BLIMP1, further represses *BCL6* and *PAX5* genes, leading to the release of *XBP1* gene suppression by PAX5. *XPB1* mRNA has to be spliced by the IRE1 endonuclease to encode for XBP1 that masters the induction of the unfold protein response (33). Pre-PBs expressed mainly *XBP1*u mRNA, and PBs and PCs expressed mainly the *XBP1*s mRNA with a 3.5- to 5-fold increase of the *XBP1s/XBP1*u mRNA ratio compared with prePBs. These data again argue for the prePB status of D4 $CD20^{low/-}CD38^{-}$ cells that start to secrete Igs, but at a weaker level than PBs or PCs, and likely exhibit a less pronounced unfold protein response. An

interesting point will be to identify the transcription factors controlling the transient *CD30* gene expression in prePBs, and then the expression of CD38 and of its ligand, CD31, in PBs. Cells with the main characteristics of these in vitro PBs could be identified in tonsils and lymph nodes at a low frequency gating on $CD19^+$ $CD20^{low/-}CD38^-$ cells. They accounted for 0.06% and 0.05% of $CD19^+$ cells in tonsils and positive lymph nodes, and they were not detected in peripheral blood and BM. We previously reported that PBs and B cells can be clearly identified by multicolor FACS analysis using cell permeabilization and anti-κ or λ Ig L chain staining (25). PBs highly express κ or λ Ig L chains, and B cells express intermediate levels. Using this technique, we found that two-thirds of these cells expressed highly cytoplasmic Ig, and the other third expressed intermediate levels characteristic of surface Ig B cells. Arce et al. (19) also detected $CD38^{low/-}$ Ig-secreting cells in tonsils, unlike peripheral blood and BM. These in vivo cells expressed cytoplasmic Igs and IL-6R, as did in vitro prePBs, unlike tonsil or lymph node B cells. CD30 could not be detected on these prePBs in vivo. This could be due to a rapid shedding of the protein in vivo following activation by CD30L (37).

Recent immunochemistry and in vivo imaging studies have documented the traffic of maturing plasma cells from GC to medullary cords in mice (9, 10). In these studies, plasma cells were documented as IgG1-producing cells, which exit the GC to the outer T cell zone in contact with $CD11c^+CD8\alpha^-$ dendritic cells producing IL-6. They then migrate randomly though linear paths in the T cell zone and join the medullary cords in contact with APRIL-producing monocytes/macrophages. These data fit well with the molecular characterization and phenotype of prePBs reported in this study. The need of T cell mimicking signals to get them in vitro suggests they are generated in the GC light zone in vivo. The loss of CXCR5 expression in prePBs should abrogate the attraction of these cells by CXCL13 producing FDC and T_{FH} and CD40L activation and promote their migration to the outer T cell zone. IL-6R expression by prePBs will prompt them to be stimulated by IL-6–producing $CD11c^+CD8\alpha^-$ dendritic cells. Of note, a removal of CD40L activation and a stimulation by IL-6 are mandatory to induce prePBs to differentiate into PBs in the current in vitro model (31), suggesting that this occurs in vivo when prePBs migrate from GC light zone to $CD11c^+CD8\alpha^-$ dendritic cells producing IL-6, which are found at the GC/T cell zone border (9). The current identification of Ig-producing prePBs, lacking CD20 and CD38, would allow for the precise location and traffic of these prePBs, compared with $CD38^+$ PBs and then $CD38^+CD138^+$ plasma cells. PrePBs also express LFA-1 (ITGAL/ITGB2) and VLA-4 (ITGA4/ITGB1) integrins that could drive plasma cell motility within lymph node through ICAM1/2 or VCAM-1 gradient (10, 38).

In conclusion, we have fully characterized a human transitional prePB stage. This opens the possibility to elucidate the mechanisms controlling their generation, to track these prePBs in the process of normal plasma cell differentiation in vivo, after immunization to a given Ag, and to look for cancer disease characterized by the immortalization of the prePBs.

Acknowledgments

We thank staff of the Microarray Core Facility and the Cytometry Platform of the Institute for Research in Biotherapy (Montpellier, France) for assistance.

Disclosures

The authors have no financial conflicts of interest.

References

1. Coffey, F., B. Alabyev, and T. Manser. 2009. Initial clonal expansion of germinal center B cells takes place at the perimeter of follicles. *Immunity* 30: 599–609.
2. Allen, C. D., T. Okada, and J. G. Cyster. 2007. Germinal-center organization and cellular dynamics. *Immunity* 27: 190–202.
3. Allen, C. D., and J. G. Cyster. 2008. Follicular dendritic cell networks of primary follicles and germinal centers: phenotype and function. *Semin. Immunol.* 20: 14–25.
4. Park, C. S., S. O. Yoon, R. J. Armitage, and Y. S. Choi. 2004. Follicular dendritic cells produce IL-15 that enhances germinal center B cell proliferation in membrane-bound form. *J. Immunol.* 173: 6676–6683.
5. Yoon, S. O., X. Zhang, P. Berner, B. Blom, and Y. S. Choi. 2009. Notch ligands expressed by follicular dendritic cells protect germinal center B cells from apoptosis. *J. Immunol.* 183: 352–358.
6. Kranich, J., N. J. Krautler, E. Heinen, M. Polymenidou, C. Bridel, A. Schildknecht, C. Huber, M. H. Kosco-Vilbois, R. Zinkernagel, G. Miele, and A. Aguzzi. 2008. Follicular dendritic cells control engulfment of apoptotic bodies by secreting Mfge8. *J. Exp. Med.* 205: 1293–1302.
7. Victora, G. D., T. A. Schwickert, D. R. Fooksman, A. O. Kamphorst, M. Meyer-Hermann, M. L. Dustin, and M. C. Nussenzweig. 2010. Germinal center dynamics revealed by multiphoton microscopy with a photoactivatable fluorescent reporter. *Cell* 143: 592–605.
8. Dogan, I., B. Bertocci, V. Vilmont, F. Delbos, J. Mégret, S. Storck, C. A. Reynaud, and J. C. Weill. 2009. Multiple layers of B cell memory with different effector functions. *Nat. Immunol.* 10: 1292–1299.
9. Mohr, E., K. Serre, R. A. Manz, A. F. Cunningham, M. Khan, D. L. Hardie, R. Bird, and I. C. MacLennan. 2009. Dendritic cells and monocyte/macrophages that create the IL-6/APRIL-rich lymph node microenvironments where plasmablasts mature. *J. Immunol.* 182: 2113–2123.
10. Fooksman, D. R., T. A. Schwickert, G. D. Victora, M. L. Dustin, M. C. Nussenzweig, and D. Skokos. 2010. Development and migration of plasma cells in the mouse lymph node. *Immunity* 33: 118–127.
11. Kabashima, K., N. M. Haynes, Y. Xu, S. L. Nutt, M. L. Allende, R. L. Proia, and J. G. Cyster. 2006. Plasma cell S1P1 expression determines secondary lymphoid organ retention versus bone marrow tropism. *J. Exp. Med.* 203: 2683–2690.
12. Radbruch, A., G. Muehlinghaus, E. O. Luger, A. Inamine, K. G. Smith, T. Dörner, and F. Hiepe. 2006. Competence and competition: the challenge of becoming a long-lived plasma cell. *Nat. Rev. Immunol.* 6: 741–750.
13. Jackson, S. M., P. C. Wilson, J. A. James, and J. D. Capra. 2008. Human B cell subsets. *Adv. Immunol.* 98: 151–224.
14. Jego, G., N. Robillard, D. Puthier, M. Amiot, F. Accard, D. Pineau, J. L. Harousseau, R. Bataille, and C. Pellat-Deceunynck. 1999. Reactive plasmacytoses are expansions of plasmablasts retaining the capacity to differentiate into plasma cells. *Blood* 94: 701–712.
15. Mei, H. E., T. Yoshida, W. Sime, F. Hiepe, K. Thiele, R. A. Manz, A. Radbruch, and T. Dörner. 2009. Blood-borne human plasma cells in steady state are derived from mucosal immune responses. *Blood* 113: 2461–2469.
16. Caraux, A., M. Perez-Andres, M. Larroque, G. Requirand, Z. Y. Lu, T. Kanouni, J. F. Rossi, A. Orfao, and B. Klein. 2011. Mobilization of plasma cells in healthy individuals treated with granulocyte colony-stimulating factor for haematopoietic stem cell collection. *Immunology* 132: 266–272.
17. Medina, F., C. Segundo, A. Campos-Caro, I. González-García, and J. A. Brieva. 2002. The heterogeneity shown by human plasma cells from tonsil, blood, and bone marrow reveals graded stages of increasing maturity, but local profiles of adhesion molecule expression. *Blood* 99: 2154–2161.
18. Caron, G., S. Le Gallou, T. Lamy, K. Tarte, and T. Fest. 2009. CXCR4 expression functionally discriminates centroblasts versus centrocytes within human germinal center B cells. *J. Immunol.* 182: 7595–7602.
19. Arce, S., E. Luger, G. Muehlinghaus, G. Cassese, A. Hauser, A. Horst, K. Lehnert, M. Odendahl, D. Hönemann, K. D. Heller, et al. 2004. $CD38^{low}$ IgG-secreting cells are precursors of various CD38 high-expressing plasma cell populations. *J. Leukoc. Biol.* 75: 1022–1028.
20. Tangye, S. G., D. T. Avery, and P. D. Hodgkin. 2003. A division-linked mechanism for the rapid generation of Ig-secreting cells from human memory B cells. *J. Immunol.* 170: 261–269.
21. Avery, D. T., J. I. Ellyard, F. Mackay, L. M. Corcoran, P. D. Hodgkin, and S. G. Tangye. 2005. Increased expression of CD27 on activated human memory B cells correlates with their commitment to the plasma cell lineage. *J. Immunol.* 174: 4034–4042.
22. Hartmann, G., and A. M. Krieg. 2000. Mechanism and function of a newly identified CpG DNA motif in human primary B cells. *J. Immunol.* 164: 944–953.
23. Jourdan, M., K. Mahtouk, J. L. Veyrune, G. Couderc, G. Fiol, N. Redal, C. Duperray, J. De Vos, and B. Klein. 2005. Delineation of the roles of paracrine and autocrine interleukin-6 (IL-6) in myeloma cell lines in survival versus cell cycle: a possible model for the cooperation of myeloma cell growth factors. *Eur. Cytokine Netw.* 16: 57–64.
24. Maecker, H. T., T. Frey, L. E. Nomura, and J. Trotter. 2004. Selecting fluorochrome conjugates for maximum sensitivity. *Cytometry A* 62: 169–173.
25. Caraux, A., B. Klein, B. Paiva, C. Bret, A. Schmitz, G. M. Fuhler, N. A. Bos, H. E. Johnsen, A. Orfao, and M. Perez-Andres; Myeloma Stem Cell Network. 2010. Circulating human B and plasma cells: age-associated changes in counts and detailed characterization of circulating normal $CD138^-$ and $CD138^+$ plasma cells. *Haematologica* 95: 1016–1020.
26. Jourdan, M., T. Reme, H. Goldschmidt, G. Fiol, V. Pantesco, J. De Vos, J. F. Rossi, D. Hose, and B. Klein. 2009. Gene expression of anti- and pro-apoptotic proteins in malignant and normal plasma cells. *Br. J. Haematol.* 145: 45–58.

27. Rème, T., D. Hose, J. De Vos, A. Vassal, P. O. Poulain, V. Pantesco, H. Goldschmidt, and B. Klein. 2008. A new method for class prediction based on signed-rank algorithms applied to Affymetrix microarray experiments. *BMC Bioinformatics* 9: 16.
28. Le Carrour, T., S. Assou, S. Tondeur, L. Lhermitte, N. Lamb, T. Rème, V. Pantesco, S. Hamamah, B. Klein, and J. De Vos. 2010. Amazonia!: an online resource to Google and visualize public human whole genome expression data. *Open Bioinformatics J.* 4: 5–10.
29. Eisen, M. B., P. T. Spellman, P. O. Brown, and D. Botstein. 1998. Cluster analysis and display of genome-wide expression patterns. *Proc. Natl. Acad. Sci. USA* 95: 14863–14868.
30. Tusher, V. G., R. Tibshirani, and G. Chu. 2001. Significance analysis of microarrays applied to the ionizing radiation response. *Proc. Natl. Acad. Sci. USA* 98: 5116–5121.
31. Jourdan, M., A. Caraux, J. De Vos, G. Fiol, M. Larroque, C. Cognot, C. Bret, C. Duperray, D. Hose, and B. Klein. 2009. An in vitro model of differentiation of memory B cells into plasmablasts and plasma cells including detailed phenotypic and molecular characterization. *Blood* 114: 5173–5181.
32. Roederer, M. 2001. Spectral compensation for flow cytometry: visualization artifacts, limitations, and caveats. *Cytometry* 45: 194–205.
33. Iwakoshi, N. N., A. H. Lee, P. Vallabhajosyula, K. L. Otipoby, K. Rajewsky, and L. H. Glimcher. 2003. Plasma cell differentiation and the unfolded protein response intersect at the transcription factor XBP-1. *Nat. Immunol.* 4: 321–329.
34. Cobaleda, C., A. Schebesta, A. Delogu, and M. Busslinger. 2007. Pax5: the guardian of B cell identity and function. *Nat. Immunol.* 8: 463–470.
35. Pridans, C., M. L. Holmes, M. Polli, J. M. Wettenhall, A. Dakic, L. M. Corcoran, G. K. Smyth, and S. L. Nutt. 2008. Identification of Pax5 target genes in early B cell differentiation. *J. Immunol.* 180: 1719–1728.
36. Calame, K. 2008. Activation-dependent induction of Blimp-1. *Curr. Opin. Immunol.* 20: 259–264.
37. Eichenauer, D. A., V. L. Simhadri, E. P. von Strandmann, A. Ludwig, V. Matthews, K. S. Reiners, B. von Tresckow, P. Saftig, S. Rose-John, A. Engert, and H. P. Hansen. 2007. ADAM10 inhibition of human CD30 shedding increases specificity of targeted immunotherapy in vitro. *Cancer Res.* 67: 332–338.
38. Luther, S. A. 2010. Plasma cell precursors: long-distance travelers looking for a home. *Immunity* 33: 9–11.